SUPPLEMENTARY INFORMATION
Self-limiting aggregation of phospholipid vesicles

N. de Lange, F. A. M. Leermakers, J.M. Kleijn

January 10, 2020

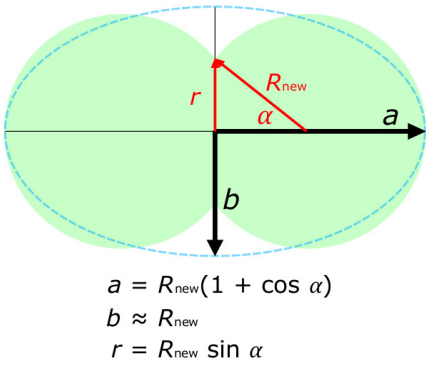

Figure S1 Vesicle pair modeled as a prolate ellipsoid with axes a, b, b with $a > b$, in order to estimate its diffusion coefficient.

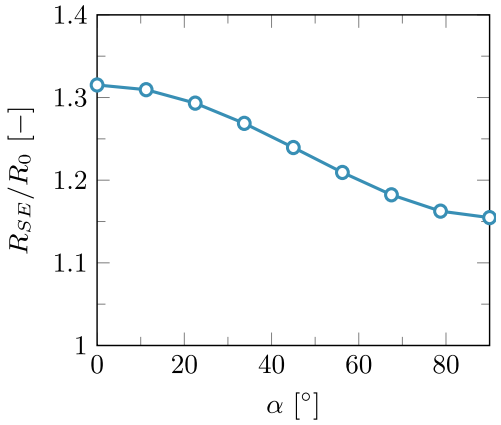

Figure S2 The Stokes-Einstein radius normalized by the radius of a single vesicle (R_{SE}/R_0) is plotted as a function of α as predicted using our simple model of vesicle pairs.

1 Overview of prepared vesicles

Vesicle preparation was performed as explained in the materials and methods section of the main document. In table S1 we present an overview of the properties of the vesicles. The S-0 vesicles are vesicles purely made from DOPC. These have been used during aggregation experiments involving C18-pNIPAm. DLS and SLS experiments involving biotin and streptavidin have been performed on B-n% samples. The FCS experiments involving biotin and streptavidin have been done using NBD-0.2% vesicles. Lastly, the PG-n% samples were used in aggregation experiments involving polylysine.

2 Simple model of vesicle pairs

We model the translational diffusion behaviour of the vesicle pairs as if they are prolate ellipsoids with axes a, b, with $a > b$. See figure S1. The translational diffusion coefficient D is given by Kuipers et al[1]

$$D = \frac{k_B T}{6\pi\eta b} \times S_{\text{prolate}} \tag{1}$$

with

$$S_{\text{prolate}} = \frac{2}{\sqrt{p^2-1}} \ln(p + \sqrt{p^2-1}) \tag{2}$$

where p is the aspect ratio: $p = a/b$. Note that S_{prolate} equals 1 in the limit of an aspect ratio of 1 and we obtain the Stokes-Einstein relation for spheres.

For the limiting case that the contact area between the two vesicles is extremely small, $a \approx 2R_0$ (R_0 being the radius of the single vesicles) and $b = R_0$, leading to $S_{\text{prolate}} = 0.76$. In other words, the diffusion coefficient D as measured with DLS would be equal to D_0/S_{prolate}. If one calculates the hydrodynamic radius from this value using the Stokes-Einstein equation (so, for a sphere with the same D), one obtains $R_{SE} = 1.32R_0$.

Generally, one can estimate the diffusion coefficient as a function of contact zone by assuming that the total area of lipid bilayer is constant:

$$A_{\text{bilayer}} = 2(4\pi R_{\text{new}}^2 - 2\pi R_{\text{new}}^2(1-\cos\alpha) + \pi r^2) \tag{3}$$

Here, the first term of the equation gives the area of the spheres with new radius R_{new}, the second term withdraws the caps from these spheres "lost" in the contact zone, and the third represents two times the contact zone. See figure S1:

We can rewrite this as:

$$A_{\text{bilayer}} = 2\pi R_{\text{new}}^2(4 - (1-\cos\alpha)^2) \tag{4}$$

This area should be equal to two times the surface area of a single vesicle, i.e.

$$A_{\text{bilayer}} = 8\pi R_0^2 \tag{5}$$

One then arrives at

$$R_{\text{new}} = \frac{2R_0}{\sqrt{4-(1-\cos\alpha)^2}} \tag{6}$$

From this, the diffusion coefficient, the Stokes-Einstein radius and the area of the contact zone can be calculated. For the case of a maximum contact zone ($\alpha = 90°$), $R_{SE}/R_0 = 1.15$ and when the contact zone is small ($\alpha = 0°$), $R_{SE}/R_0 = 1.32$, See figure S2. As our experiments show that $R_h/R_0 \approx 1.4$ for vesicle pairs we conclude that the contact areas are small.

3 Vesicle collision and lateral diffusion timescale calculations

The vesicle collision time can be calculated using the following equation:

$$\tau = d^2/6D_v \tag{7}$$

Table S1 Properties of the various vesicles in 50 mM NaCl

Vesicle Code	Membrane composition [DOPC/DOPE-Biotin/ DOPG/NBD-PE]	Radius [nm] ± St. Dev.	PDI [-] ± St. Dev.
S-0	1 / 0 / 0 / 0	76.5 ± 2.8	0.16 ± 0.05
B-0.04%	999 / 1 / 0 / 0	75.6 ± 0.9	0.11 ± 0.04
B-0.2%	995 / 5 / 0 / 0	74.6 ± 1.1	0.11 ± 0.03
B-0.4%	990 / 10 / 0 / 0	73.5 ± 0.9	0.11 ± 0.04
B-0.6%	985 / 15 / 0 / 0	75.1 ± 1.1	0.10 ± 0.03
PG-2.5%	975 / 0 / 25 / 0	64.6 ± 1.4	0.10 ± 0.04
PG-10%	900 / 0 / 100 / 0	72.6 ± 1.7	0.09 ± 0.04
NBD-0.2%	980 / 10 / 0 / 10	69.6 ± 1.3	0.12 ± 0.04

where D_v is the vesicle diffusion coefficient and d the average distance between vesicles. These parameters can be calculated as follows:

$$D_v = k_B T / 6\pi\eta R_v \tag{8}$$

and

$$d = \langle r \rangle - 2R_v \tag{9}$$

with k_B the Boltzmann constant, T the temperature in Kelvin, and R_v the vesicle radius; $\langle r \rangle$ is the mean center-to-center inter-particle distance, which in turn can be calculated using the molar vesicle concentration C_v:

$$\langle r \rangle = 1/C_v^{1/3} \tag{10}$$

With our experimental parameters, ($C_v \approx 5 \times 10^{-10}$ M, $R_v \approx 65$ - 80 nm and $T = 298$ K we find a collision time of $\sim 80 - 130$ ms. The diffusion time for a biotinylated lipid to diffuse over the maximum distance d_b to the contact area of a vesicle pair is given by:

$$t_{\text{diff}} = d_b^2 / 4D_l \tag{11}$$

where D_l is the lateral diffusion coefficient of a lipid in the bilayer and d_b corresponds to half the circumference of a vesicle. Using the same experimental parameters and a $D_l \approx 8.25 \times 10^{-12}$ m^2/s, we find diffusion times of $1 - 2$ ms.

4 DLS and SLS data analysis

The DLS and SLS data analysis has been previously described in literature[2–4]. The following sections provide a short overview of the equations used to calculate the main properties of our system including the fits of the correlation curves that correspond to values of table 1 in the main article.

4.1 Cumulant analysis of DLS data

The light scattering intensity as obtained with DLS or SLS can be described as a constant average scattering intensity I with a time-dependent part $I(t)$. The intensity autocorrelation function $G_2(\tau)$, correlating the scattering intensity at time t with the intensity at time $t + \tau$, can be described as follows:

$$G_2(\tau) = \frac{\langle I(t) \cdot I(t+\tau) \rangle}{\langle I(t) \rangle^2} \tag{12}$$

The corresponding field autocorrelation function $G_1(\tau)$ can be related to $G_2(\tau)$ using the Siegert equation and can be rewritten as follows:

$$G_1(\tau) = \frac{1}{\sqrt{\beta}} \sqrt{G_2(\tau) - 1} \tag{13}$$

where β is an experimental constant that depends on the DLS/SLS setup and has a value approximately equal to unity. $G_1(\tau)$ can also be written as a weighted average of all possible decays dependent on the correlation decay rate Γ, diffusion coefficient D of the particles and the wave vector q:

$$G_1(\tau) = \lim_{n\to\infty} \frac{1}{n} \sum_{i=1}^{n} w_i(\Gamma_i) e^{-\Gamma_i \tau} \tag{14}$$

with $\Gamma = q^2 D$ and $q = \frac{4\pi n}{\lambda_0} \sin\left(\frac{\theta}{2}\right)$. Here, λ_0 is the wavelength, n is the refractive index of the medium and θ is the detection angle.

For monodisperse spherical particles, the above equations can be combined, which leads to

$$\ln\sqrt{G_2(\tau) - 1} = \ln(A) - \Gamma\tau \tag{15}$$

with $A = \sqrt{\beta}$. By plotting the experimentally obtained $\ln\sqrt{G_2(\tau) - 1}$ as a function of τ, we obtain a linear relation from which Γ and $\ln(A)$ can be calculated.

For polydisperse samples, the size distribution can be fitted through the cumulant expansion[2]. As in our case the second order cumulant and third order cumulant fits resulted in similar results for the found diffusion coefficients, the second order cumulant was used to fit all the data presented in the article. This second order cumulant is expressed as:

$$\ln\sqrt{G_2(\tau) - 1} = \ln(A) - \Gamma\tau + \frac{\mu_2}{2!}\tau^2 \tag{16}$$

which is effectively is equation (15) but with an extra term $\frac{\mu_2}{2!}$. We calculated D from Γ and subsequently used the Stokes-Einstein relation for spherical particles to calculate the hydrodynamic radius (R_h):

$$R_h = \frac{k_B T}{6\pi\eta D} \tag{17}$$

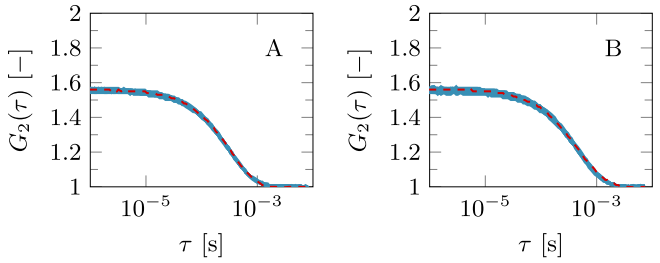

Figure S3 The first twenty autocorrelation curves for NBD-0.2% vesicles without added streptavidin (A) and with added streptavidin ($N_s/N_b = 1/25.6$) (B) as obtained using DLS. A single fit is optimized for all autocorrelation curves (red dashed line).

where k_B is the Boltzmann constant, T is the absolute temperature and η is the viscosity of the solvent. For our calculations, $T = 293$ K and $\eta = 8.90 \times 10^{-4}$ Pa s are used, corresponding to water at 25 ° C. The polydispersity index of the vesicles is calculated as:

$$\mathrm{PDI} = \frac{\mu_2}{\Gamma^2} \tag{18}$$

The first 5 fits of the second cumulant analysis of the DLS results in table 1 in the main article are shown in figure S3.

For our data analysis, we assume the vesicles to be spherical, which is actually not true for vesicle pairs and higher forms of aggregation. For a simple model of vesicle pairs and how it relates to the Stokes-Einstein radius of single vesicles, we refer back to section 2 of this document.

4.2 CONTIN Analysis

The cumulant method is valid provided that we are dealing with a Gaussian distribution around a single population. To check this, we performed a CONTIN analysis[5,6] on our DLS data. This method uses a multi exponential fit with n fractions with n up to about 100 fractions:

$$G_1(\tau) = \frac{1}{n}\sum_{i=1}^{n} w_i(\Gamma_i) e^{-\Gamma_i \tau} \tag{19}$$

with $w_i(\Gamma_i)$ the weighting function showing how much the particles in size range i contribute to the intensity of the scattered light. We subsequently plotted the acquired data as an "equal area representation"[7], giving $w_i(\Gamma_i) \cdot \Gamma_i$ normalized to the maximum weight, as a function of R. An overview of this analysis for representative aggregation experiments using all three different linkers is found in figure S4

Figure S4 shows that a distribution around a single particle size is found for all aggregation experiments. In addition, the radii obtained at the peak values of these size distributions are similar to those obtained from the cumulant method. We therefore conclude that the cumulant method is sufficient to analyse the DLS results obtained during the aggregation experiments.

We also found a significant broadening of the vesicle size distribution for PG vesicles upon addition of PLL. This suggests that at an average aggregation of 2, a broad distribution between single vesicles, vesicle pairs, trimers etc is obtained. In contrast, for both the biotin-streptavidin and C18-PNIPAM linker systems the peaks in the size distributions shift to higher radii as a result of aggregation. This is because of the migration of biotinylated lipids or PNIPAM-C18 to the contact zones which causes vesicle pairs to form more selectively during the aggregation experiment.

4.3 Guinier analysis from SLS data

In a Guinier analysis the natural logarithm of the Rayleigh scattering, $\ln(\mathrm{R}_\theta)$, is plotted as a function of the wave factor squared (q^2) as obtained through multi-angle measurements. For a homogeneous, stable particle solution, the curve follows a linear relationship. See figure S5 for some representative results for the B-0.4% vesicles at different stages of the aggregation experiment.

Each curve is a linear relationship according to the following equation:

$$\ln(R_\theta) = \ln(K_R C M) - \frac{R_g^2}{3} q^2 \tag{20}$$

with K_R a constant (see equation below) and C the mass concentration of our sample which is known (generally $C = 0.075$ kg/m^3) and also constant. The molar mass (M_w) can be calculated from the intercept and the radius of gyration (R_g) is calculated from the slope.

$$K_R = \frac{4 n_m^2 \pi^2}{\lambda_0^4 N_{Av}} \left(\frac{dn}{dC}\right)^2 \tag{21}$$

Here n_m is the refractive index of the solvent, λ_0 is the wavelength of the light in vacuum, and $\frac{dn}{dC}$ is the refractive index increment)

The mean aggregate number (M) is calculated by dividing the average molar mass of the aggregates by the average molar mass of the single vesicles: (M_0):

$$M = \frac{M_w}{M_0} \tag{22}$$

4.4 Fitting of the form factor

When examining a dispersion of particles using light scattering, light that emits from different parts of a particle can lead to interference of the scattered light. This interference partially extincts the scattered light, resulting in a lower Rayleigh ratio (R_θ). The reduction of R_θ is described by the form factor (P), which is a function of the wave vector (q) and the radius of the particle (R). By fitting the form factor to the static light scattering data (R_θ as a function of q) we can obtain the radius (R) of our vesicles. While the fitting of the form factor is an alternative way to calculate the radius of particles, in our aggregation experiments this method is not very suited as the form factor equation needs to be adapted to the shape of the particles, which differs between vesicles, vesicle-pairs and higher forms of aggregation, and is not accurately known. For this data analysis, we assumed all particles to consist of spherical hollow shells for which the thickness of the shell (i.e. the membrane) is infinitely thin. The form factor can then be simplified to the following equation:

$$P(qR) = \left(\frac{sin(qR)}{qR}\right)^2 \tag{23}$$

The results of this fit for 3 stages during our aggregation experiment with biotin and streptavidin can be found in figure S6.

As can be seen from the figure, we can fit the data of individual vesicles much better compared to the data obtained at conditions in which we have vesicle pairs or higher forms of aggregation, reflected by much higher residuals for these conditions compared to individual vesicles. While we cannot accurately estimate the correct radius of our particles using this approach, the results indicate that vesicles during the aggregation experiments do not fuse to form larger vesicles, since if that was the case, fits of the form factor of a hollow spherical shell would hold better.

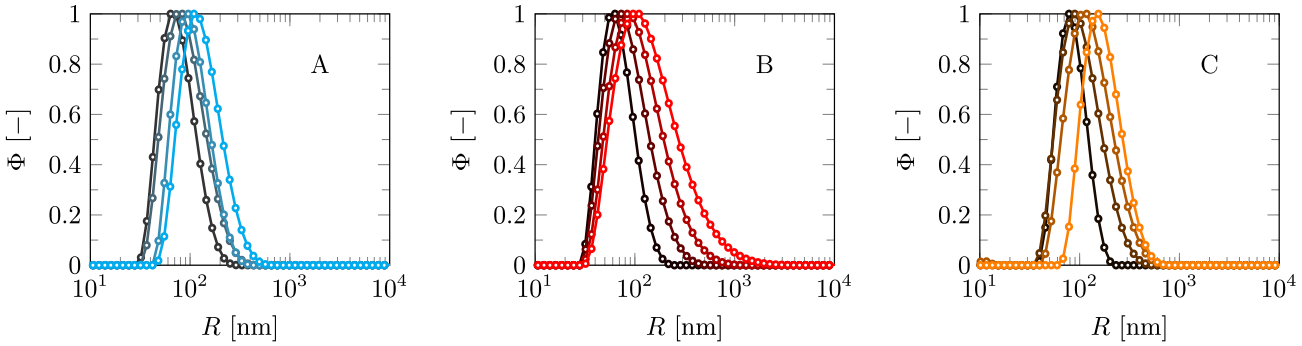

Figure S4 Particle size distribution curves obtained using a CONTIN analysis on DLS data for different aggregation experiments. (A) Aggregation of biotinylated vesicles ($f_b = 0.0004$) using streptavidin. From dark to light blue: $N_s/N_b = 0$, $N_s/N_b = 1/102.4$, $N_s/N_b = 1/12.8$, $N_s/N_b = 1/1.6$. (B) Aggergation of PG vesicles ($f_{\mathrm{DOPG}} = 0.1$) using PLL at 10 mM NaCl. From dark to light red: $N_{\mathrm{PLL}}/N_v = 0$, $N_{\mathrm{PLL}}/N_v = 0.75$, $N_{\mathrm{PLL}}/N_v = 1.5$, $N_{\mathrm{PLL}}/N_v = 2.12$. (C) Aggregation of S-0 vesicles using C18-pNIPAm. The graphs contain data as measured at 40 °C. From dark to light orange: $f_{\mathrm{C18-pNIPAm}} = 0$, $f_{\mathrm{C18-pNIPAm}} = 0.02$, $f_{\mathrm{C18-pNIPAm}} = 0.04$, $f_{\mathrm{C18-pNIPAm}} = 0.16$. The graphs are plotted as an "equal area representation", i.e. $\Phi = w_i\Gamma_i \times \Gamma_i / \left(w_i\Gamma_i \cdot \Gamma_i\right)_{\max}$ as a function of R (logarithmic scale).

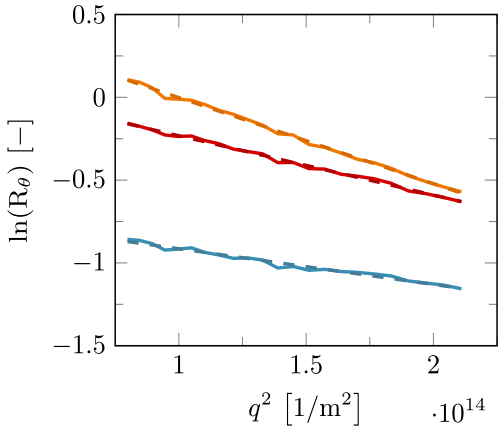

Figure S5 Guinier plots of the multi-angle SLS measurements at different stages of the aggregation experiment of B-0.4% with subsequent addition of streptavidin. Representative curves are shown for conditions at $N_s/N_b = 0$ (blue), $N_s/N_b = 1/12.8$ (red) and $N_s/N_b = 1/1.6$ (orange). Both the measurements (solid lines) as the linear fit (dashed lines), representing equation (19), are shown.

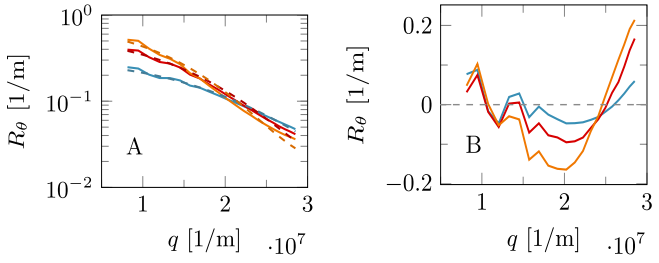

Figure S6 Form factor fits, fitted according to equation (22), of our multi-angle SLS experiments are shown (A), including the residuals of the fit (B). The measurement was performed at scattering angles ranging from 30° to 130°. Measurements are shown corresponding to three conditions during our aggregation experiment with B-0.4% vesicles with subsequent addition of streptavidin: $N_s/N_b = 0$ (blue), $N_s/N_b = 1/25.6$ (red) and $N_s/N_b = 1/1.6$ (orange). Both measured data (solid lines, A) and the form factor fits (curved lines, A) are shown. The fits are optimized to that the sum of residuals is minimal.

5 FCS data analysis

In this section we provide a short overview of the equations used to fit the correlation curves obtained from FCS measurements. The approaches used to calculate the main properties of our system, like the average number of fluorescent particles in the confocal volume $\langle N \rangle$ and the diffusion coefficient (D), can be found in literature[3,8].

The fluorescence intensity as obtained with FCS can be described as a constant average fluorescence intensity I with a time-dependent part $I(t)$. The autocorrelation function $G(t)$, correlating the fluorescence intensity at time t with the intensity at time $t+\tau$, can be described as:

$$G(\tau) = \frac{\langle I(t) \cdot I(t+\tau) \rangle}{\langle I(t) \rangle^2} = \frac{\langle I \rangle^2 + \langle \Delta I(t) \cdot \Delta I(t+\tau) \rangle}{\langle I \rangle^2} \tag{24}$$

The autocorrelation curves that are obtained can be fitted with

$$G(\tau) = 1 + \frac{1}{\langle N \rangle}\left(1 + \frac{F_{\mathrm{trip}}}{1 - F_{\mathrm{trip}}}\right) \cdot e^{-t/T_{\mathrm{trip}}} \cdot \sum_{i=1}^{n} \frac{F_i}{(1 + t/\tau_{\mathrm{diff,i}}) \cdot \sqrt{1 + (\omega_{xy}/\omega_z)^2 \cdot t/\tau_{\mathrm{diff,i}}}} \tag{25}$$

Properties in this equation not yet described are F_{trip}, which accounts for the fraction of molecules in the triplet state and T_{trip} which is the average time a molecule resides in the triplet state. The last part of the equation describes the diffusion behavior of the molecules, where F_i is the fraction of species, i, with diffusion time $\tau_{\mathrm{diff,i}}$; ω_{xy} and ω_z are the equatorial and axial radii of the detection volume, respectively. See figure S7 for the fit of the correlation curves corresponding to the results as displayed in table 1 in the main article.

The diffusion coefficient D_i of species i is directly related to the observed diffusion time $\tau_{\mathrm{diff,i}}$, according to

$$D_i = \frac{\omega_{xy}^2}{4 \cdot \tau_{\mathrm{diff,i}}} \tag{26}$$

The hydrodynamic radius (R_h) for the vesicles, can be calculated using the Stokes-Einstein equation for spherical particles, see equation 17.

The mean aggregate number (M) for FCS is calculated by dividing the average number of single vesicles in the confocal volume

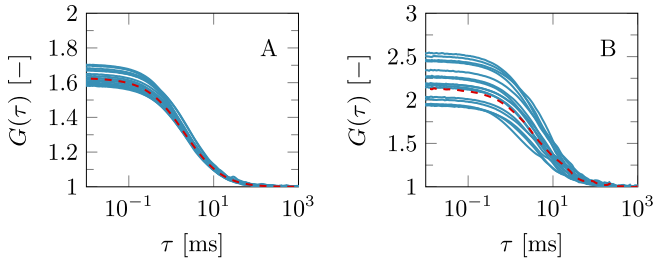

Figure S7 FCS autocorrelation curves for NBD-0.2% vesicles without added streptavidin (A) and with added streptavidin ($N_s/N_b = 1/25.6$) (B). A single fit according to equation (24) is optimized for all autocorrelation curves (red dashed line).

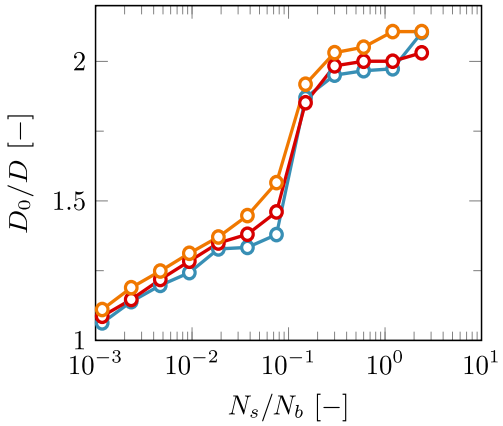

Figure S8 Normalized hydrodynamic radius of vesicles with $f_b = 0.01$ as a result of stepwise adding streptavidin. Results for various vesicle concentrations are shown: $C_v \sim 2.0 \times 10^{-10}$ M (blue), $C_v \sim 5.0 \times 10^{-10}$ M (red) and $C_v \sim 2.5 \times 10^{-9}$ M (orange).

($\langle N_0 \rangle$) by the actual average number of particles in the confocal volume ($\langle N \rangle$).

$$M = \frac{\langle N_0 \rangle}{\langle N \rangle} \tag{27}$$

For our data analysis, we assume the vesicles to be spherical, which is actually not true for vesicle pairs and higher forms of aggregation. For a simple model of vesicle pairs and how it relates to the Stokes-Einstein radius of single vesicles, we refer back to section 2 of this document.

6 Effect of vesicle concentration on aggregation of vesicle pairs using biotin and streptavidin

The aggregation of the vesicles as a function of N_s/N_0 is independent of the vesicle concentration: see figure S8. From this result it can be concluded that our experiments are in the regime where the collision time between vesicles is much higher than the diffusion time of biotin-bound streptavidin to existing contact zones: if the collision time would be comparable or smaller than the lipid diffusion time, aggregation beyond vesicle pairs would increase with increasing vesicle concentration, until eventually uncontrolled aggregation would occur, as found by Kisak et al[9].

7 Vesicle aggregation for small polylysine

Controlled aggregation of vesicles using small PLL molecules (M_n of 1 - 5 kg/mol) was practically not achieved. Adding a small amount of PLL did not lead to any aggregation, see figure S9A.

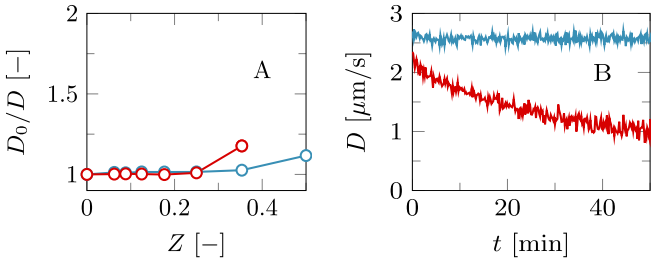

Figure S9 Normalized diffusion coefficient of vesicles as a function of Z, the ratio between positive charges, due to polylysine, and negative charges, due to DOPG (A). The experiment is performed for PG-5% vesicles (red), and for PG-10% vesicles (blue). Small polylysine (M_n of 1 - 5 kg/mol) are subsequently added to the vesicle solution. The diffusion coefficient as measured with DLS is shown as a function of time after adding small polylysine to the solution (B). Here, results of PG-5% vesicles are shown at a $Z = 0.35$ (blue) and a $Z = 0.5$ (red). Note that the blue curve in B represents the last data point of the red curve in A.

Increasing the amount of PLL in the solution, had no effect until uncontrolled complete aggregation occurred. This is illustrated in figure S9B by the progressive decline of the diffusion coefficient when $Z = 0.5$ (red curve), while for $Z = 0.35$ (blue curve) (represents the last data point of the red curve of figure S9A) the diffusion coefficient D remained stable.

We assume that the cause for this behaviour is related to the gradual adsorption of small PLL molecules to the vesicle surface. In low concentrations they absorb only a little as the conformational and translational entropy penalty upon binding to a vesicle is too high, while the entropy gain of released counterions compensates only just for this. The adsorption increases slowly with concentration and as soon as they do adsorb significantly so that they can induce bridging, the concentration of freely dispersed PLL molecules is sufficiently high so that these can replenish the chains that are lost in the contact zones. In contrast, for large PLL molecules strong adsorption already occurs at very low PLL concentrations such that the adsorption and subsequent bridging results in a decline of the PLL concentration in the bulk. This depletion of freely dispersed chains prevents further adsorption on the freely exposed vesicle surfaces, simply because the PLL chains are not available: for large PLL chains all chains are adsorbed and virtually no chains remain in the bulk. In other words, short PLL chains with a finite bulk concentration have a buffering capacity for adsorption, while longer chains with a vanishing bulk concentration lack this buffering capacity. In this explanation the surface-to-volume ratio is essential.

8 Electrophoretic mobility of PG vesicles

In addition to DLS and SLS, the electrophoretic mobility (μ_e) was measured to check for potential neutralization of DOPG vesicles by PLL addition. See figure S10 for the results.

As can be seen from figure S9A, μ_e remains constant with increasing Z ($N_{\mathrm{PLL}}/N_{\mathrm{DOPG}}$). This could mean that no PLL adsorbs to the vesicle surface at all, leading to no aggregation of vesicles. This is the case for $f_{\mathrm{DOPG}} = 0.025$ and $C_{\mathrm{NaCl}} = 100$. However, for other conditions, our DLS and SLS measurements clearly show an increase in aggregate size, indicating that for these conditions PLL does adsorb onto the surface of the vesicles. We anticipate that PLL is completely enclosed within the contact area of vesicle pairs or aggregates. It is therefore not present in the slipping plane of the aggregates and thus has practically no effect on μ_e.

The mobility μ_e is depending on the salt concentration (C_{NaCl})

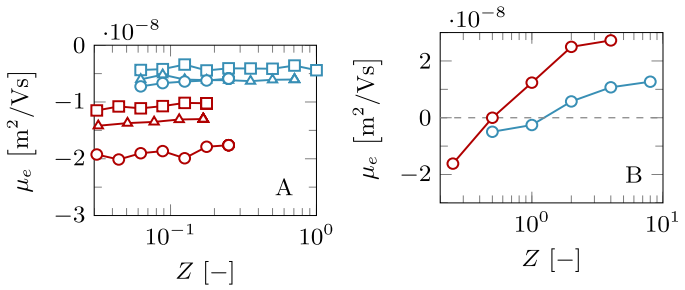

Figure S10 Electrophoretic mobility results for the aggregation experiments involving PG vesicles and PLL. Aggregation experiments with stepwise addition of PLL, up until uncontrolled aggregation occurred (A) (corresponding to the DLS data of figure 3 in the main document), as well as aggregation experiments in which PLL is added in one go (B) are shown. Blue: vesicles with a DOPG lipid fraction $f_{\mathrm{DOPG}} = 0.025$. Red: $f_{\mathrm{DOPG}} = 0.1$. Measurements were performed at three NaCl concentrations: 10 mM (circles), 50 mM (triangles) and 100 mM (squares).

or vesicle charge density (σ) though. A higher σ, caused by an increasing fraction of DOPG in the vesicles, increases the absolute mobility ($|\mu_e|$) of vesicles, while a higher C_{NaCl} decreases it. Interestingly, $|\mu_e|$ is still higher at high σ with a high C_{NaCl}, compared to low σ at low C_{NaCl}, which supports the notion that the electrostatic interaction between PLL and vesicles is still very high for high σ with a high C_{NaCl} and thus the effect of salt concentration on the extent of vesicle aggregation is not yet visible.

Although we observed a continuous increase in aggregate size for $Z \approx 1$ and size measurements are therefore unreliable, electrophoretic mobility measurements still gives us much insight. It is expected that μ_e changes sign at $Z \approx 1$, as was previously reported [10]. To confirm this, we performed additional zeta potential measurements of vesicles in which a substantial amount of PLL is added in one go, see figure S9B. We indeed observe a change in sign, which indicates that for $Z \approx 1$ PLL is not fully enclosed in contact areas.

Notes and references

[1] B. Kuipers, M. Van de Ven, R. Baars and A. Philipse, *Journal of Physics: Condensed Matter*, 2012, **24**, 245101.

[2] D. E. Koppel, *The Journal of Chemical Physics*, 1972, **57**, 4814–4820.

[3] A. Nolles, A. H. Westphal, J. A. de Hoop, R. G. Fokkink, J. M. Kleijn, W. J. van Berkel and J. W. Borst, *Biomacromolecules*, 2015, **16**, 1542–1549.

[4] A. Guinier and G. Fournet, *Small-Angle Scattering of X-rays*, 1955.

[5] S. W. Provencher, *Computer Physics Communications*, 1982, **27**, 229–242.

[6] S. W. Provencher, *Computer Physics Communications*, 1982, **27**, 213–227.

[7] P. Stepanek, *The Method and Some Applications*, 1993, 177–241.

[8] V. V. Skakun, M. A. Hink, A. V. Digris, R. Engel, E. G. Novikov, V. V. Apanasovich and A. J. Visser, *European Biophysics Journal*, 2005, **34**, 323–334.

[9] E. Kisak, M. Kennedy, D. Trommeshauser and J. Zasadzinski, *Langmuir*, 2000, **16**, 2825–2831.

[10] D. Volodkin, V. Ball, P. Schaaf, J.-C. Voegel and H. Mohwald, *Biochimica et Biophysica Acta (BBA)-Biomembranes*, 2007, **1768**, 280–290.